EFDA–JET–PR(12)15

M. Graham, M.-L. Mayoral, I. Monakhov, J. Ongena, T. Blackman, M.P.S. Nightingale, E. Wooldridge, F. Durodié, A. Argouarch, G. Berger-By, A. Czarnecka, S. Dowson, R. Goulding, S. Huygen, P. Jacquet, T.J. Wade, E. Lerche, P.U. Lamalle, H. Sheikh, D. Van Eester, M. Vrancken, A. Walden, A. Whitehurst and JET EFDA contributors

Implementation of Load Resilient ICRF Systems to Couple High Levels of ICRF Power to ELMy H-Mode Plasmas in JET

Implementation of Load Resilient ICRF Systems to Couple High Levels of ICRF Power to ELMy H-Mode Plasmas in JET

M. Graham[1], M.-L. Mayoral[1], I. Monakhov[1], J. Ongena 2), T. Blackman[1], M.P.S. Nightingale[1], E. Wooldridge[1], F. Durodié[2], A. Argouarch[3], G. Berger-By[3], A. Czarnecka[4], S. Dowson[1], R. Goulding[5], S. Huygen[2], P. Jacquet[1], T.J. Wade[1], E. Lerche[2], P.U. Lamalle[2], H. Sheikh[1], D. Van Eester[2], M. Vrancken[2], A.Walden[1+], A. Whitehurst[1]
and JET EFDA contributors*

JET-EFDA, Culham Science Centre, OX14 3DB, Abingdon, UK

[1]EURATOM-CCFE Fusion Association, Culham Science Centre, OX14 3DB, Abingdon, OXON, UK
[2]LPP-ERM/KMS, Association "Euratom-Belgian State", 1000 Brussels, Belgium, TEC Partner
[3]CEA, IRFM, F-13108 Saint-Paul-lez-Durance, France.
[4]Association EURATOM-IPPLM, Hery 23, 01-497, Warsaw, Poland.
[5]Oak Ridge National Laboratory, Oak Ridge, United States
[+]Deceased December 2007
** See annex of F. Romanelli et al, "Overview of JET Results",*
(23rd IAEA Fusion Energy Conference, Daejon, Republic of Korea (2010)).

Preprint of Paper to be submitted for publication in
Plasma Physics and Controlled Fusion

ABSTRACT.
The paper summarizes the continuous developments made to the Ion Cyclotron Radio Frequency (ICRF) system at JET in order to improve the reliability of the power coupled to plasma. It details the changes and improvements made to the system so that more power is coupled during ELMy plasmas as well as increasing the power density to demonstrate reliable operation in the range of the requirements for ITER. Results obtained using the conventional matching (stubs and trombones) system, 3dB couplers and the conjugate-T scheme with variable matching elements outside the wave launching structure (External Conjugate-T or ECT) and inside the wave launching structure (ITER Like Antenna or ILA) are described. The presence of the 3 different approaches to load resilient ICRF systems at JET creates a unique opportunity to compare these methods under very similar plasma conditions and to assess the results of ICRF power delivery to ELMy plasmas, an important issue for ITER. The impact of the availability of increased levels of reliable ICRF power on plasma physics studies in JET is illustrated.

1. INTRODUCTION

The Ion Cyclotron Resonant Frequency (ICRF) system at JET has continually developed with the aim of reliably coupling large amounts of power into plasmas with fast varying load conditions (due to ELMs, pellets injection, MHD instabilities in the plasma edge, etc.). The development of load tolerant ICRF systems are essential not only for the JET research program but also for future systems such as ITER, DEMO and other fusion reactors based on magnetic confinement.

The first ICRF system installed in JET in 1984 consisted of two prototype short pulsed (1-2s) antennas (so called A0 antennas) [1], consisting of two current conductors (straps) each, with each strap fed by a 1.5MW amplifier. After successful testing, which included paralleling amplifiers using a 3dB coupler system [2], these antennas were upgraded to the so called A1 antennas which were able to handle the increased 20s pulse length requirements [3]. The final fully installed system consisted of eight A1 antennas with each strap fed by an Eimac 8973 1.5MW tetrode. In the period 1988 to 1990 the endstage cabinets were redesigned and upgraded for the installation of 2MW Thompson TH525 tetrodes. The system at this time consisted of sixteen similar circuits operating in the frequency range 23 to 57 MHz and powered the original eight 2 strap antennas (Fig 1).

The highly reactive antenna strap impedance, also referred as antenna loading, depends on the plasma Scrape-Off-Layer (SOL) density profiles and the antenna design. A matching circuit to transform the antenna loading (typically between 1 and 3 Ohm) to an impedance suitable for the RF sources (30Ω for JET's RF sources) is then necessary. At the time of the A0 antennas, variable stubs and trombone transmission line elements were utilised to perform this transformation. Initially, at low power, a 200 kHz frequency sweep was used to find a match. The stubs and trombones were then manually adjusted before decreasing the sweep and increasing the power. The introduction of the automatic matching system in 1989 [4], which adjusted the position of the stub, the length of the trombone in real time and provided real time control of small frequency shifts around the

operating frequency, allowed the ICRF system to deliver quickly and reliably the ICRF power on a large variety of plasma loads.

An alternative matching system, using a motorised capacitor tuning stub 2.6m from the antenna, was installed and tested in 1987 [5]. The tuning stub demonstrated an improvement in generator tolerance to large plasma loads; however, because of its position, it could only be operated at two close frequencies near 34MHz

The matching system, still using the stub and trombones [6], continued to demonstrate successful multi-megawatt performance (up to 22MW [7]) on limiter plasmas with stationary or slowly evolving SOL properties.

In 1994 the sixteen transmission lines feeding the eight two straps antenna arrays were reconfigured to feed four new A2 antenna arrays, consisting each of four straps and labelled A, B, C and D (Fig.1). Each A2 antenna [2] is fed by a corresponding module consisting of two 4MW generators (Fig.2). The A2 antenna was required because to the change in plasma shape (especially the up-down asymmetry) resulting from the installation of the JET divertor.

The introduction of the divertor in JET allowed long duration H-mode plasma operation to be established with associated Edge Localised Modes (ELMs) [8]. These ELMs cause very fast load variations to the ICRF antennas. Although during ELMs the loading increases as the density close to the antenna increases, this variation is too fast (sub-millisecond) for the mechanical tuning elements to react (seconds) and whilst the frequency matching system is very fast, it only counteracts changes to the imaginary part of the load and cannot fully adjust the system to its optimum parameters [9]. The insufficient intrinsic load tolerance and the slow response of the mechanical matching circuits causes the power reflected to the RF generators to reach unacceptable levels and subsequently trigger protective power trips.

Indeed, the standard JET technique, as described in section 3.1, for protecting the RF sources, transmission lines and antennas relies on monitoring the Voltage Standing Wave Ratio (VSWR) at the generator, a measure for the mismatch between the load and the RF source. A long power trip time for arcs is required (~20-50ms) to allow the arc to extinguish and local vacuum conditions to recover prior to reapplication of RF power, while for ELMs a shorter trip time (~ 1ms) is sufficient. Unfortunately, this protection system cannot distinguish between a fast reflection occurring for example during ELMs and an arc. This means that as a result, the capability of the ICRF system is unnecessarily reduced due to the large 'power-off' time during discharges with frequent ELMs. Typically, the total ICRF pulse time is reduced by 50-70% and the averaged coupled power reaches ~20-30% of the set power as clearly illustrated in Fig.3.

In the next section of this paper, we will present the load tolerant systems that were tried and review the achievements of the ones currently implemented i.e. the 3dB hybrid couplers and the External Conjugate-T. Note that the achievements of the ITER-like antenna, also "load tolerant", will be only briefly mentioned and we will refer the reader for more details to the paper by F. Durodie et al. in this special issue [10]

In order to alleviate these problems in the new load tolerant systems, additional arc detection protection had to be incorporated and these are reviewed in section 3 of this paper. Finally in section 4 we will give an overview of the plasma scenarios that have been used over the past few years and the new capability of the JET ICRF systems i.e. the 8MW of ICRF power on type I ELMs H-mode.

2. DEVELOPMENT OF LOAD TOLERANT SYSTEMS WITH CONVENTIONAL JET ICRF ANTENNAS

2.1. OVERVIEW

To allow the RF sources to remain matched through these fast load transients seen by the plasma facing antennas, new matching systems have been developed, implemented and tested over the years in JET.

(i) Following the pre-matching capacitive stub work [5], a wideband SLiding IMPedance matching system (SLIMP) was introduced in 1998 [11]. The SLIMP (Fig.4), a high impedance 105 Ω adjustable section in between two 24Ω one meter adjustable sleeves, was installed into each transmission line at a distance of 18.5m from the antenna and was expected to deliver broadband matching at 28, 36, 44 and 52MHz. By setting the positions for the stub, trombone and SLIMP, the load variations were expected to be converted into a phase variation of the reflection coefficient, Γ, and the generator VSWR could be kept low by the adjustment of the frequency, using the fast frequency feedback system. As the system was however very sensitive to the electrical distance between the SLIMP starting point and the antenna short-circuit, and also very difficult to set up and run [12], no further development was carried out and the system is no longer used.

(ii) In 2004-2005 the 3dB coupler system was installed to feed both the JET antenna arrays A and B and is based on the principle of diverting the reflected power, occurring during load transients (e.g. caused by ELMs), to a dummy load [13] (Fig.5). This approach was also proven experimentally on ASDEX-Upgrade [14] and is presently adopted as the main option for ITER. It provides steady operational conditions for the RF generators during symmetric load transients caused by fast disturbances in the edge, (i.e. the two straps that are connected using the 3dB hybrid coupler undergo the same change in loading), as the reflected power is diverted to the dummy loads. Therefore, at the expense of wasting a small fraction of the generated power during such fast events to the dummy loads, (much) more power can be delivered to the plasma: e.g. in the case of ELMs the ASDEX-Upgrade team estimates that between 7 and 8% on average of the generated power was lost in the dummy load [15].

(iii) The Conjugate-T (CT) concept [16, 17] consists of pairs of straps connected to a T-junction. Impedance transformation elements are inserted in each branch of the T-junction such that the two branches have complex conjugate admittances, thus eliminating the susceptance at the T-junction. (Fig.6). The target impedance at the Conjugate-T point, Z_{CT}, is typically between 3 and 6 Ω and does not vary during fast load changes. A 2nd stage matching,

between the T-junction and the generator and made up of stub and trombone tuners, which transforms the low Z_{CT} value to Z_0 ($Z_0 = 30\Omega$ at JET). Two distinct ways of implementing this concept have been developed at JET.

1. In 2007 an External Conjugate-T (ECT) system was implemented on antenna arrays C and D (see Fig 7) [18] after the successful proof of principle demonstration on half of array C [19]. In the case of the External Conjugate-T system, trombones in the transmission lines connecting the T-junction to the straps of Antennas C and D are used to adjust the T-junction impedance. The previously installed SLIMPs were converted into trombones to facilitate the matching requirements for ECT.
2. In parallel with the ECT installation, the ITER Like Antenna (ILA) was installed (see Fig 7) which implemented the conjugate-T arrangement by the use of variable capacitors mounted inside the wave launching structure. These capacitors are not easily accessible and in the case of failure are hard to replace. The target impedance at the Conjugate-T point can be adjusted for a reference plasma loading condition to minimize the variations of ZCT to plasma load due to e.g. ELMs. The 2nd stage matching, made of stub and trombone tuners, transforms the low ZCT value to Z0 (Z0 = 30W at JET). In the case of asymmetries in the two branches of the T-junction (due to geometry or plasma effects) the ZCT can have a small reactive part in order to equalize the voltages in both straps. More details on this antenna can be found in [10].

The present layout of the current ICRF system at JET is schematically shown in Fig. 7. The system involving module C and D can be configured in either the conventional way or in ECT mode. Note that when the ECT system is in use, module C is not used and therefore the total power available from the RF plant is reduced. Despite this, the total ICRF power delivered to ELMy plasmas on JET, using the three remaining modules, is higher than with the original (fig 2) system as will be shown below.

2.2. STEADY AND INCREASED LEVELS OF ICRF POWER USING THE 3DB HYBRID SYSTEM.

Using the 3dB hybrid system, the reflected power occurring during ELMs was indeed successfully directed to the 3dB's load instead of the generator (see fig 8) [13].

An example of the improvement in the coupled power, P_A, P_B, P_C and P_D, is illustrated in Fig. 9, where one can see clearly the difference between the power delivered on an ELMy plasma by antenna A and B equipped with a 3dB hybrid coupler and that delivered by antenna C and D, configured in the conventional way, thus not tolerant to ELMs. The strongly decreased number of trips for A and B allows the generators to continue to deliver power into the ELMy plasma and leads to a significant increase in averaged coupled power. So far, up to 3.3MW of steady ICRF power during ELMy mode was coupled by module B (see examples on Fig.10 and Fig.11)

The 3dB hybrid coupler system however, imposes a few restrictions:

- The phase of the current on the 4 straps of the antenna arrays can be adjusted to various phase configurations (e.g. 0, p, 0, p for heating or 0, +p/2, +p, +3p/2 for co or counter current drive phasing). However, the output ports of the 3dB hybrid couplers to individual straps of antenna arrays A and B have a fixed difference of p/2, which is key to the diversion of the reflected power to the load port rather than the source port (Fig. 5). The length of the transmission lines to the 2 powered straps paired by the 3dB hybrid coupler cannot be changed to correct this phase difference. The antenna arrays A and B are "phase coupled", cannot be independently operated, and therefore will always have the same phasing configuration.
- Detrimental effects to the LH coupling are seen during combined operation of ICRF on antenna array B and LH, due to the close proximity of this antenna to the LH launcher [20]. Previously, when antenna arrays A and B were independently operated, antenna array B could be switched off, however, with the installation of the 3dB hybrid coupler this is no longer possible and if the 3dB system is used power is equally delivered to both antenna arrays A and B.

  Attempts to minimise the interference of antenna array B on LH by the powering of only one antenna array, by mismatching one of the outputs of the 3dB hybrid system has been investigated. However, this is limited, because the total reflected power no longer goes to the load but is instead distributed between the load and the output of the amplifier which in turn can trip the system. Experiments, used to limit the power to antenna array B because of the ICRH interference with the 3.7GHz microwave system known as the Lower Hybrid (LH) system, have established the degree of mismatch the system can tolerate before the system trips [20].

2.3. DELIVERY OF STEADY HIGH LEVELS OF ICRF POWER TO JET USING THE ECT SYSTEM.

The commissioning of the External Conjugate-T (ECT) on conventional antennas C and D has revealed its robust and reliable performance [18]. Simultaneous matching of all four ECT circuits has been successfully achieved under a variety of antenna loading conditions including vacuum, L-mode plasmas with 'sawtooth' activity and ELMy H-mode plasmas with mid-plane limiter-separatrix distances in the range of 4-14 cm. The implemented real-time control algorithms have proven stable and effective during changing experimental conditions.

The ECT has been fully commissioned at four frequencies of 32.5 MHz, 42.5 MHz, 46.0 MHz and 51.0 MHz covering the majority of JET operational scenarios. Most of the experiments were performed at standard $(0,\pi,0,\pi)$ phasing of the antenna straps; transition to alternative phasings, such as $\pm(0,\pi/2,\pi,3/2\pi)$ and $(0,\pi,\pi,0)$ have been found to be straightforward and since 2009 the ECT system has been routinely used during ICRF operations at JET.

Experiments in ELMy plasma conditions have confirmed the expected high load-tolerance of

the ECT system. During all types of ELMs, the VSWR value has remained well below the VSWR protection trip threshold of 3 traditionally used at JET. As illustrated in Fig.12, this allowed trip-free amplifier operations and continuous power injection even during large ($\Delta W_{DIA} \leq 0.7$MJ) Type-I ELMs (Fig.12a) accompanied by strong changes of the antenna resistive (Fig.12b) and inductive loading (Fig.12c). Depending on the JET plasma scenario, the trip-free time average power levels delivered to ELMy H-mode plasmas by the ECT system reached 4MW (Fig.13). The observed momentary increase in the power levels coupled to plasma during ELMs (Fig.12e) is explained by a reduction of the power losses in the long transmission lines during high loading conditions.

As with the 3dB hybrid couplers, the ECT imposes a phase relationship of the antenna straps that are fed from the Conjugate T point (CT): this is the key to the load tolerant properties of the circuit and can either be close to 0 or to π, depending on the loading and the transmission line lengths between the straps and the CT. Therefore in order to keep the flexibility in the choice of the phasing of the 4 strap arrays, the ECT circuits have been connected between similar straps of two different strap arrays on modules C and D. Hence the antenna arrays C and D are "phase coupled" and their phasings cannot be independently operated. However, this relies on the load variations being nearly identical on the two antenna straps.

2.4. OPERATIONAL EXPERIENCE WITH THE ILA ANTENNA

Operation of the ILA on a range of plasma configurations and antenna frequencies demonstrated the ITER-relevant use of a high power density conjugate-T configuration.

The capability of operation at 42kV and electric fields of 2.5kV/mm in L-mode as well as H-mode was shown. This is regardless of the orientation with respect to the magnetic field on JET and without observable degradation of the pulse quality inherent to voltage handling.

Maximum achieved coupled power in L-Mode with the ILA alone was 4.8MW, (resulting in 6.2MW/m^2 [11]), an increase by a factor of about 4 in power density compared to what previously was obtained with the A2 antennae. In H-Mode a maximum coupled power of 1.88MW was achieved (power density of 4.1MW/m^2). Examples of the power coupled from the ILA to ELMy H-mode are shown in Fig.10 and Fig.16. An important result noted during ILA operations is that the impurity production is comparable or lower with that for the A2 antennas but at power densities up to 4 times higher as illustrated in Fig.14 [21].

Higher powers could not be reached on L-mode plasmas due to control limitations of the RF power plant. The development of full ILA array operation on H-mode plasma was curtailed due to the premature failure of an antenna vacuum capacitor.

Control of the antenna matching elements in the presence of high mutual coupling between straps during simultaneous use of the four conjugate-T systems in the ILA antenna proved feasible but is quite sensitive on H-mode plasmas due to the lower coupling and did require the development of additional pulse analysis software tools to set the 2nd stage matching circuit to maximize the load tolerance [22]

Finally, the experiment also allowed validation of the coupling code TOPICA to predict the performance of an ICRF launcher for ITER. For more information on the ILA see the paper by F. Durodie et al. in this special issue [10]

3. ARC DETECTION SYSTEMS

Arc detection systems are critical to the operation of any high power RF system as they prevent unwanted arcing and subsequent damage to components. Below are details of the main systems which have been tried and implemented on JET.

3.1. ARC DETECTION USED FOR THE NORMAL MATCHING CONFIGURATION

On JET, the main protection against arcs is based on the Voltage Standing Wave Ratio, VSWR, which is related to the reflection coefficient, ρ, through the formula

$$\mathrm{VSWR} = (1 + \rho)/(1 - \rho)$$
$$\text{where } \rho = |V_{\text{reflected}} / V_{\text{forward}}|.$$

$V_{\text{reflected}}$ and V_{forward} are the reflected and forward voltage wave amplitudes measured using directional couplers installed on the transmission lines.

The VSWR is thus a measure for the matching conditions of the monitored section of transmission line and for a matched transmission line this VSWR is close to 1 (i.e. the voltages are nearly equal anywhere along the transmission line and the reflected voltage wave is much smaller than the forward voltage wave). An increase of the VSWR is due to either the changed loading conditions of the antenna (e.g. due to ELMs which the matching system has not yet corrected for) or an arc appearing in the transmission line, matching or antenna system. For reasons of safety and protection of the generators, arcing is always assumed and the RF power source is tripped, i.e. the power is momentarily removed as fast as possible (typically 10–20μs) and reapplied after a short delay which would allow time for a supposed arc to extinguish and the conditions in the vicinity of the presumed arc to restore to normal (e.g. surface temperature of the conductors, quality of the vacuum, etc.). The trip time varies from 20ms down to 5ms, depending on the trip repetition frequency, and has a recovery time of 10 to 80ms.

3.2. ARC DETECTION USED FOR THE 3DB HYBRID SYSTEM.

The use of 3dB hybrid system to obtain load tolerance requires a relaxation of the VSWR protection limits on part of the system, in order to prevent power trips due to the effect of the substantial variations in the VSWR which remain present in the transmission lines connecting the matching stubs to the 3dB couplers. If arcs occur in one branch of the 3dB system then this in turn causes an asymmetry which subsequently causes a mismatch the generator feed port, potentially leading to a power trip triggered by the VSWR protection in the Output Transmission Line (OTL as defined in

figure 5). Instances of simultaneous arcs on both 3dB branches which cancel the reflected power at the generator port, although rare, have been observed on DIII-D [23] so that inferring the presence of arcs based on the detection of asymmetries supposedly caused by arcs, is not infallible.

Two different VSWR systems are utilised for safe operation of the antennas with 3dBs [13], as follows:

- Firstly, the OTL VSWR protection is set to a ratio of 2.4:1 using the directional couplers for the forward and reflected power on the OTL in between the generator and the 3dBs couplers (Fig.5). These couplers are used to provide the voltage reflected ($V_{reflected(OTL)}$) and forward (Vforward(OTL)) signals to give $\rho_{OTL} = |_{Vreflected(OTL)} / V_{forward(OTL)}|$.

- Secondly, the VSWR protection can be set at different ratios of 3:1, 5:1, 10:1 and 15:1 using the directional couplers for the forward and reflected power in the Splitter Transmission Line (STL) (Fig. 5) These couplers provide the voltage reflected ($_{Vreflected(STL)}$) and forward ($V_{forward(STL)}$) signals to give $\rho_{STL} = |V_{reflected(STL)} / V_{forward(STL)}|$.

During operation on ELMs, the VSWR trip level on the STL is set to its highest values, in order to allow higher reflected powers during ELMs without tripping the system and still providing some level of arc protection. An example of arc detection using this system is illustrated in Fig.8. During ELMs, the coupling resistance increases (Fig.8b) and reflections are present in both STLs connected to the A and B antenna straps (Fig.8c). These reflected signals however are combined in the 3dB hybrid coupler and directed to the load (Fig.8e), and therefore do not propagate to the generator (Fig.8d). The generator is not tripped and continues to deliver power to the system.

Another issue is the possible occurrence of arcs at low voltage points i.e. voltage nodes [24] that are difficult to detect. Such arcs are presumed to be due to gas from current overheating which allows a discharge to start. These can occur in the vacuum transmission line (VTL) and cannot be detected, particularly if a high VSWR set ratio has been set. An example of an arc that does not cause the VSWR protection to trip the system is illustrated in Fig.15. The figure demonstrates that after the second ELM shown in this picture, the coupling resistance and VSWR in the STL connected to strap 2 of antenna A return to the pre-ELM level. This is not the case for the STL connected to strap 2 of antenna B. Both signals show a marked increase compared to the pre-ELM level. However, no trip is generated as the VSWR protection ratio for the STL in this case was set to 15:1 and similarly no trip is generated in the OTL as the VSWR protection ratio in this case is 3:1. This generator continues to deliver the requested output power for about 150ms until another event occurs that finally causes a trigger and a shutdown of the generator. Following the observation of such an event the OTL VSRW level was decreased to 2.4:1.

Operations using the VSWR settings of above 10:1 at 37 and 42MHz have to be carefully monitored using the fast data acquisition as there is a potential risk of serious damage on the bellows

situated in the vacuum transmission line [13]. At these frequencies the voltage nodes are located at bellows in the transmission line and sustained arcing in this area would result in a vacuum leak and the subsequent unavailability of the 3dB hybrid system antennas.

3.3. ARC DETECTION USED FOR THE ECT SYSTEM

In order to operate the ECT configuration safely, a novel arc detection strategy, in addition to the conventional VSWR system, has been developed and implemented. The Advanced Wave Amplitude Comparison System (AWACS) [18], [25] monitors the ratios of the reflected voltage on the Output Transmission Line (OTL) to the forward voltages on the transmission lines after the conjugate-T, CTL and DTL (Fig. 6) The threshold values for these ratios, $\rho_{CTL} = |V_{reflected(OTL)}/ V_{forward(CTL)}|$ and $\rho_{DTL} = |V_{reflected(OTL)}/ V_{forward(DTL)}|$, can be changed and are selectable between $\rho = 0.6, 0.7, 0.8$ and 0.9. During arcs the parallel impedance of the line seen at the T-junction increases, thus causing the current going to the arcing branch to drop. The voltage $V_{reflected(OTL)}$ increases and that for $V_{forward(CTL)}$, and $V_{forward(DTL)}$ decreases, rendering the measured ratios very sensitive to arcing in one of the branches of the ECT system. This is not the case during ELMs. The AWACS system is therefore highly sensitive to arcing in the CTL and DTL but tolerant to ELMs [18], [25]

3.4. ARC DETECTION FOR THE ILA

Arc and ELM detection was also a challenge for the ITER Like Antenna (ILA) and in this case two different systems were implemented and tested to overcome these difficulties:

(i) Scattering Matrix Arc Detection [26] or SMAD is based on a redundancy check of the real-time measured voltages and currents close to the T-junction. The SMAD system has become fully functional under a variety of plasma loading conditions and has allowed the ILA to couple power safely into ELMy H-mode plasmas.

(ii) The Sub Harmonic Arc Detection or SHAD [27] based on the detection of characteristic frequencies below the antenna frequency which are caused when arcs are present. The SHAD system on JET, while detecting all the arcs, was also triggered by many false positives, caused by parasitic signals e.g. ion cyclotron emission, fast particle modes etc. This renders the system difficult to use and more efforts would be needed to make this a more reliable system on JET [28]

3.5. OPTICAL ARC DETECTION SYSTEM

An optical arc detection system was installed on the Vacuum Transmission Line (VTL) to try and detect arcs within the vacuum section of the ICRF transmission lines. The system consists of a mirror, an optical fibre arrangement and a detector. (Fig 16). Initial tests proved to be unsuccessful and further investigations were carried out. Tests on an identical spare detector demonstrated that at low light intensities the image becomes significantly blurred, due to scattered light from the walls of the detector tube. Given the very low light levels involved with arcing it was concluded that

any scattering of the light on the walls of the tube makes the signal too difficult to detect. Further investigations which improve the design e.g. designing a shortened route from arcing point to detector still have to be undertaken.

4. RECENT PROGRESS OBTAINED WITH THE HIGH POWER AVAILABLE FROM ALL LOAD RESILIENT ICRF SYSTEMS AT JET

Up to 7MW has been delivered by the simultaneous use of the ECT and the 3dB systems (see Fig.13) where both systems performed equally well under ELMy conditions [18]. Increasing the power levels injected into plasma by the A2 antenna systems above 7MW will require more conditioning efforts to allow reliable operation at voltages exceeding 30kV. The ILA has achieved 1.88MW using only half of the antenna array into ELMy plasmas. The full array is clearly capable of achieving more power, but this will require further experiments. The availability of higher ICRF power levels has allowed good progress to be obtained in several interesting physics questions. An overview of studies that benefited from increased levels of ICRF power available on JET is presented here.

Comparison of the performance of NBI dominated to ICRF heating (ICRH) dominated discharges and possible consequences for the ITER Q = 10 operational scenario was performed [30]. A level of ICRF power up to 8.3MW was reached using simultaneously the A2 ICRF ELM-resilient systems and the new ILA antenna. Central H minority heating (4-5% H_2 in D_2) was used with a magnetic field B_t of 2.7T, an ICRF frequency of 42MHz and a dipole antenna phasing and a typical discharge is shown in Fig.10. Although previous comparisons of ICRF and NBI heated H-modes consistently reported no difference in the energy confinement enhancement factor, H_{98} ([29]), the number of ICRH dominated Type I ELMy H-modes in the JET database was limited due to the difficulties in coupling ICRF power in the presence of ELM.

The aim of the new experiment was to compare pedestal/ELMs, core confinement and transport of Type I ELMy H-modes with ICRF and NBI heating, in a relevant H-mode operational space in terms of plasma current, Ip (= 2.5MA), q_{95} (=3.6) and density (= 60-70% of the Greenwald density nG). The range of power deposition profile, ion to electron power deposition, core fuelling and momentum injection explored in the experiment were inclusive of what is expected for ITER in the baseline H-mode scenario.

The overall comparison of the confinement of H-modes with NBI and with combined heating at different fractions (≥50%) of ICRF power, different levels of total power and different density showed that the thermal energy confinement enhancement factor H_{98} did not depend on the heating mix. The power deposition profiles varied from very peaked (~85% power inside $\rho = 0.5$) with predominant ICRH, to flat deposition for pure NBI cases. The plasma toroidal rotation was varied by a factor of ~5 in the core and ~10 in the edge. Those variations did not produce any significant difference in the density and temperature profiles or in the global confinement. Pedestal pressure and width were also found to be independent of heating mix. The response of the global confinement to changes in density and power, and the consequent variations of H_{98}, were the same for ICRH or

NBI dominated discharges and reflected the changes in pedestal pressure.

The results indicated that the global confinement scaling at the basis of the ITER Q=10 performance prediction is robust in spite of having being derived from a majority of plasma H-modes with high momentum input, prevalent ion heating and relatively flat deposition profiles, and provided further confidence in the robustness of the predictions for ITER [29]. More information on these experiments can be found in Reference 30.

Over 8MW of ICRF power could also be coupled to Advanced Scenarios. H_2 minority heating in D_2 plasmas at 42MHz was used with a small amount of gas dosing (4×10^{21} el/s to 7.4×10^{21} el/s). This amount of ICRF power together with ~20MW of NBI power, resulted for the first time in record performances in Advanced Scenarios at B_t=2.65 T in JET under steady state conditions (i.e. for time intervals greater than 10 confinement time) with the following characteristics: $H_{98} = 1.2$, total and thermal β_N of 2.7 and 2.0 respectively, a ratio of the averaged ion temperature to the averaged electron temperature $\langle T_i \rangle / \langle T_e \rangle = 1.05$ at a global normalized Larmor radius $\rho^*/\rho^*_{ITER} \sim 2$, normalized collisionality $\nu^*/\nu^*_{ITER} \sim 4$ (see a typical discharge on Fig. 11). Interpretative modelling showed that in such plasmas with central electron temperatures of about 8keV at an electron density of 5 10^{19} cm^{-3} (Fig. 17), the fraction of bootstrap current was 40-45% . This compares favorably with the ITER Steady-State scenarios where the following requirements must be met: ~50% bootstrap current fraction, high normalised beta, total $\beta_N \approx 3$ and thermal $\beta_N \approx 2.4$, and $H_{98} \approx 1.4$-1.5. Thus, the availability of high levels of load resilient ICRF power brought the JET plasma performance closer to the ITER Steady State targets. More information on these important experiments can be found in [31].

The availability of increased levels of ICRF power compared to the capabilities of the original A2 ICRF system at JET also allowed extended investigations of ion heat transport. Although for these studies the plasmas were mainly L-Mode ones, the higher level of ICRF power allowed for larger excursions in the ion heat flux (of about a factor 2) than were previously possible. The heating scheme used was the (^{3}He) minority scheme in D_2 plasmas with a ^{3}He concentration of about 8% allowing localized ion power deposition with short slowing down times, which is ideally suited for ion temperature modulation experiments. An outstanding question was the behaviour of ion stiffness (resilience of the ion temperature profile to changes in the plasma conditions) in conditions of low rotation, i.e. low NBI power. The impact of rotation on ion stiffness was then studied by comparing low rotation high ICRF power plasmas with high rotation high NBI power plasmas. In this way the coupling between heat and torque sources, which is characteristic of most JET plasmas, could be broken and the effect of rotation studied in a clean way. An important result [32] was that the presence of strong rotation shear under conditions of low magnetic shear is mitigating the level of ion stiffness, allowing higher central T_i peaking. This then suggested that improved core confinement in Advanced Scenarios (nearly exclusively obtained with very high levels of NBI) could be caused by the mitigation of ion stiffness due to the presence of high levels of rotation and a broad region of low magnetic shear. These results also imply that some degree of rotational shear should

be established in ITER in order to obtain Advanced scenarios. In addition, the high ICRF power now available also allowed studies of the role of the ratio T_e/T_i on ion heat transport, specifically on the value of the critical ion temperature gradient for the onset of ITG turbulence. Previously a strong influence of T_e/T_i on confinement was found, but always in experiments characterized by high rotation and coupling between T_e/T_i and rotation. In JET the value of T_e/T_i was scanned in conditions of low rotation, using mainly ICRF power either in H minority (for electron heating) or in ^{3}He minority (for ion heating). The dependence of the ITG threshold on T_e/T_i was found rather mild and in agreement with linear gyro-kinetic theory predictions, thus suggesting that previous results may have been polluted by variations of T_e/T_i and rotation.

CONCLUSION

The implementation of load resilient ICRH systems in JET over the past years has allowed over 8MW of ICRH power to be coupled to ELMy H-Mode plasmas. This has been obtained by the simultaneous use of the ITER Like Antenna (ILA) with internal matching Conjugate-T, the 3dB Hybrid Couplers and the External Conjugate T system on the A2 Antennas. Due to the failure of one of the inner capacitors in the ILA, the antenna is currently not in use.

The use of load resilient antenna systems also required additional arc detection systems to be developed and various novel solutions to be implemented. An extension of the traditional VSWR arc detection systems was necessary when using the 3dB coupler system in order to provide additional VSWR protection on the output of the 3dB couplers. For the ILA, the SHAD (Sub Harmonic Arc Detection), SMAD (Scattering Matrix Arc Detection) have been developed and tested with success, although the SHAD still requires further development. Arc detection for the ECT led to the development of AWACS (Advanced Wave Amplitude Comparison System), which proved to be very effective in detecting actual arcs. An optical arc detection system has also been tested in the Vacuum Transmission Lines of the ICRH system, but this did not perform satisfactorily, and further research is required to optimize the results.

High ICRF power levels have allowed extended comparisons of the quality of NBI dominantly heated and ICRF dominantly heated ELMy H-Mode plasmas, and showed that the confinement performance of the discharges is independent of the heating mix, for the range of plasma conditions explored. These results provide further confidence in the ITER Q=10 baseline scenario. Increasing levels of ICRF to Advanced Scenarios led to plasmas with the highest normalized beta β_N and H_{98} factor ever reached at high magnetic field (B_t=2.65T). The availability of high levels of load resilient power thus brought also the performance of JET Advanced Scenarios closer to the ITER Steady State Targets.

ACKNOWLEDGEMENTS

This work, supported by the European Communities under the contract of Association between EURATOM and CCFE, was carried out within the framework of the European Fusion Development

Agreement. The views and opinions expressed herein do not necessarily reflect those of the European Commission. This work was also part-funded by the RCUK Energy Programme under grant EP/I501045. The authors would like to thank Roberta Sartori (Fusion For Energy Joint Undertaking, Spain), Paola Mantica (ENEA-CNR, Italy) and Joelle Mailloux (EURATOM/CCFE Fusion Association, UK) for their contributions to the last paragraph.

REFERENCES

[1]. P.P. Lallia et al., Proc. 5th Topical Conference on Radio-Frequency Plasma Heating, Madison, Wisconsin, Feb 21-23 (1983), Paper B-I.1, pp. 126-129

[2]. T.J. Wade et al., Fusion Engineering and Design **24** (1994) 23-46.

[3]. A.S. Kaye et al., Proc. 11th Symposium on Fusion Engineering (SOFE), Austin, Texas, Nov 18-22 (1985), Vol.**2**, 1204-1209.

[4]. G. Bosia et al., Proc. 16th Symposium on Fusion Technology (SOFT), London, United Kingdom, Sept 3-7 (1990) 1099-1103.

[5]. T.J. Wade et al., Proc. 12th Symposium on Fusion Engineering (SOFE), Monterey, Oct 12-16 (1987), 1200-1203.

[6]. G. Bosia et al., Proc. 15th Symposium on Fusion Technology (SOFT), Utrecht, Netherlands, Sept 19-23 (1988), Vol.**1**, 459-463.

[7]. T.J. Wade et al., Proc. 14th Symposium on Fusion Engineering (SOFE), San Diego, California, Sept 30 – Oct 3 (1991), Vol.2, 902-907.

[8]. D. Campbell et al., Plasma Phys. Control Fusion, 38 (1996) 1497

[9]. J-M. Noterdaeme et al., Fusion Engineering and Design **74**, 191-198 (2005).

[10]. F. Durodié et al., "Operational experience with the ICRF ITER like antenna on JET", this issue

[11]. M. Simon et al., Proc. of 2nd Topical Conf. on Radio Frequency Heating and Current Drive of Fusion Devices (Brussels, 1998) 105

[12]. P.U. Lamalle, Proc, 24th EPS Conf. on Controlled Fusion and Plasma, Berchtesgaden (Germany) Europhysics Conference Abstracts, Vol. 21A Part I (1997) 133

[13]. M.-L. Mayoral, et al., 17th Top. Conf. on RF power in Plasmas, AIP Conf. Proc. 933 (2007) 143

[14]. J-M. Noterdaeme et al., 13th Top. Conf. on RF power in Plasmas, AIP Conf. Proc. 485 (1999) 92

[15]. V. Bobkov, Institut für Plasmaphysik, Max-Planck Institut, ASDEX-team, Garching, private communication.

[16]. T.J. Wade, private communication / JET internal memo 1998

[17]. G. Bosia, High-power density ion cyclotron antennas for next step applications, Fusion Science and Technology **43** (2003) 153–160.

[18]. I. Monakhov, 18th Top. Conf. on RF power in Plasmas, AIP Conf. Proc. 1187 (2009) 205-208

[19]. I. Monakhov, et al., Fusion Engineering and Design **74**, 467-471 (2005).
[20]. K. Kirov et al., Plasma Physics and Controlled Fusion **51**, 044003 (2009)
[21]. A. Czarnecka et al., "Impurity production from the ICRH antennae in JET", this issue.
[22]. M. Vrancken et al., 18th Top. Conf. on RF power in Plasmas, AIP Conf. Proc. 1187 (2009) 225
[23]. R. Goulding, ORNL, private communication.
[24]. I. Monakhov et al., 17th Top. Conf. on RF power in Plasmas, AIP Conf. Proc. 933 (2007) 151
[25]. I. Monakhov et al., 17th Top. Conf. on RF power in Plasmas, AIP Conf. Proc. 933 (2007) 147
[26]. M. Vrancken et al., Proc. 26th Symposium on Fusion Technology (SOFT), Porto, Portugal, Sept 27 - Oct 1 (2010), Fusion Engineering and Design **86** (2011) 522
[27]. F. Braun et al., Proc. 19th Symposium on Fusion Technology (SOFT), Lisbon, Portugal, Sept 16-20 (1996), 601-603
[28]. P. Jacquet et al., 19th Top. Conf. on RF Powers and Plasmas, AIP Conf. Proc. 1406 (2011) 21
[29]. ITER Physics Basis, Nuclear Fusion **39**, 2175 (1999)
[30]. T.W. Versloot et al. Nuclear Fusion **51** (2011) 103033
[31]. J. Mailloux et al, 23rd IAEA Fusion Conference, Daejeon, paper EXC/1-4 (2010)
[32]. P. Mantica et al., Plasma Physics Control. Fusion **53** (2011) 124033

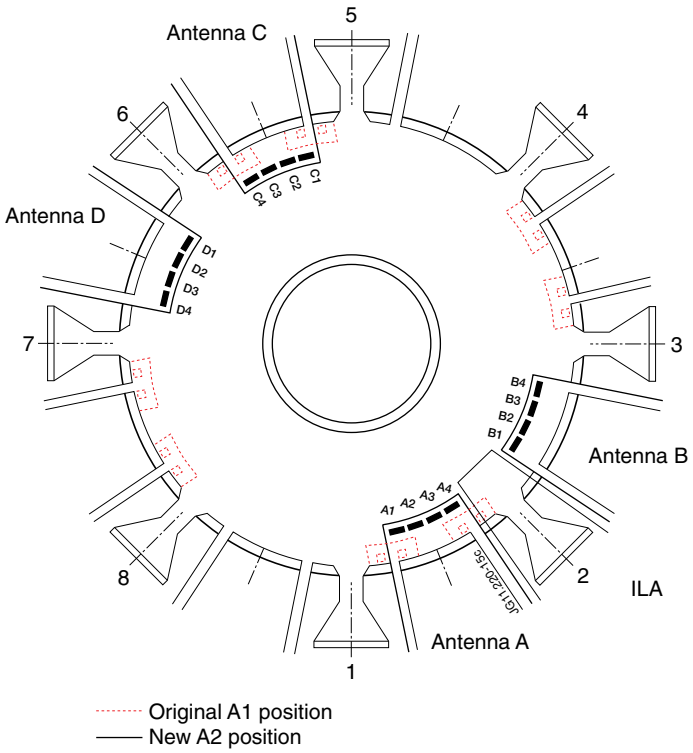

Figure 1: Layout of the ICRF antennas in the JET torus for the A1 antennas (dotted red), A2 antennas and ITER like Antenna (ILA).

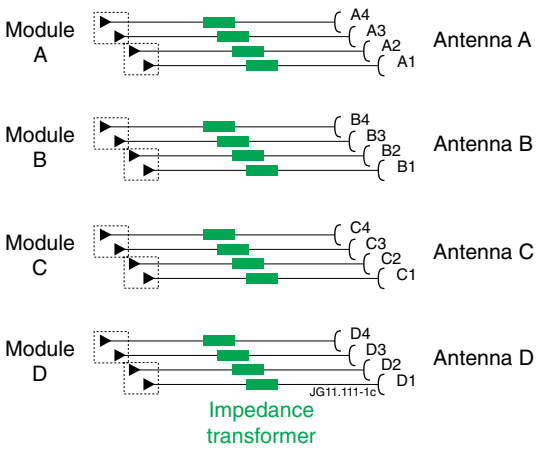

Figure 2: The JET ICRH system before recent modifications, with the conventional antennas A, B, C and D, consisting each of 4 straps (labelled 1 to 4) individually fed by one amplifier. Two amplifiers (of 2MW each) are combined in one generator (dashed boxes). Two generators combine to one module with a total of 8MW generated power.

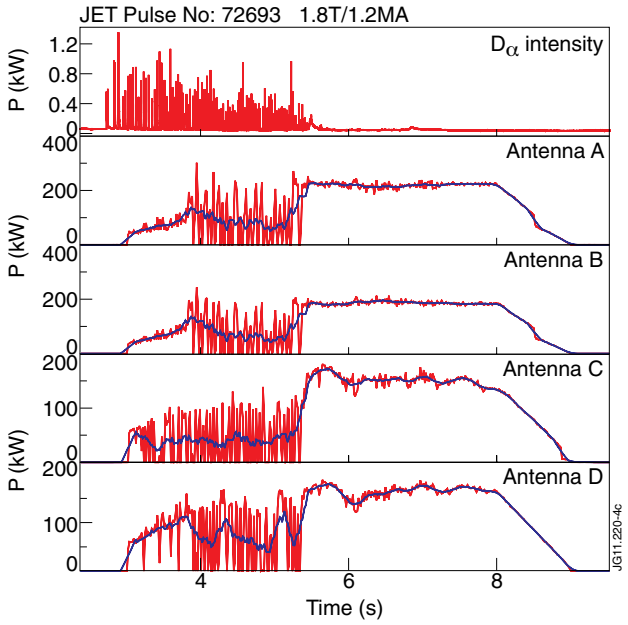

Figure 3: Illustration of the sensitivity of the conventional A2 antennas to fast load changes as e.g. due to ELMs. Red lines represent the instantaneous power coupled to the plasma; blue lines represent the average power. During the ELMy phase of this H-mode plasma the load changes cause frequent trips of the arc protection system leading to a low average value for the coupled power.

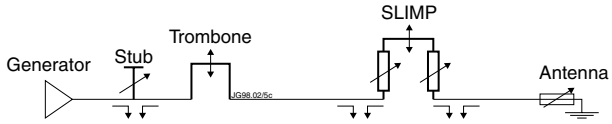

Figure 4: Schematic representation of the JET transmission lines including the Sliding Impedances (SLIMP).

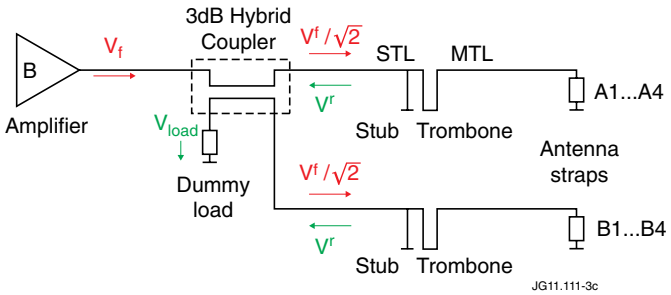

Figure 5: The load resilient 3dB system on JET showing the Output Transmission Line (OTL), Splitter Transmission Line (STL) and Main Transmission Line (MTL) connected to the A2 antenna arrays A and B. The output power of the RF amplifier is split in 2 and sent to pairs of straps of antenna A and B. The reflected power is combined in the coupler and sent to the dummy load and thus never reaches the generators.

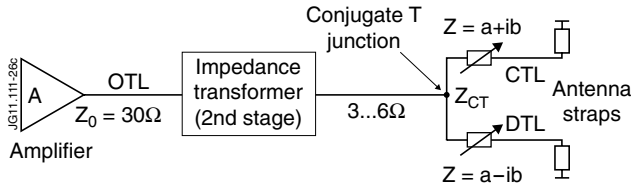

Figure 6: Load resiliency using the Conjugate-T matching principle. After the Output Transmission Line (OTL) and impedance transformer, a variable impedance is added between the T junction and the antenna straps. The sum of the conductances appearing at the T junction will vary little while the sum of the susceptibilities will keep cancelling, resulting in load resilience for the total circuit.

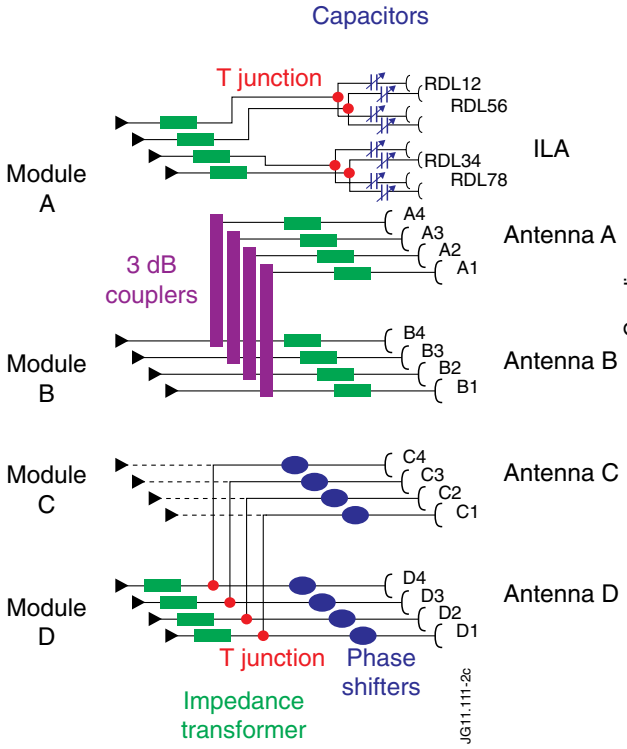

Figure 7: The current JET system after recent modifications to test various load resilient ICRH antenna options: ITER Like antenna, 3dB couplers and External Conjugate T.

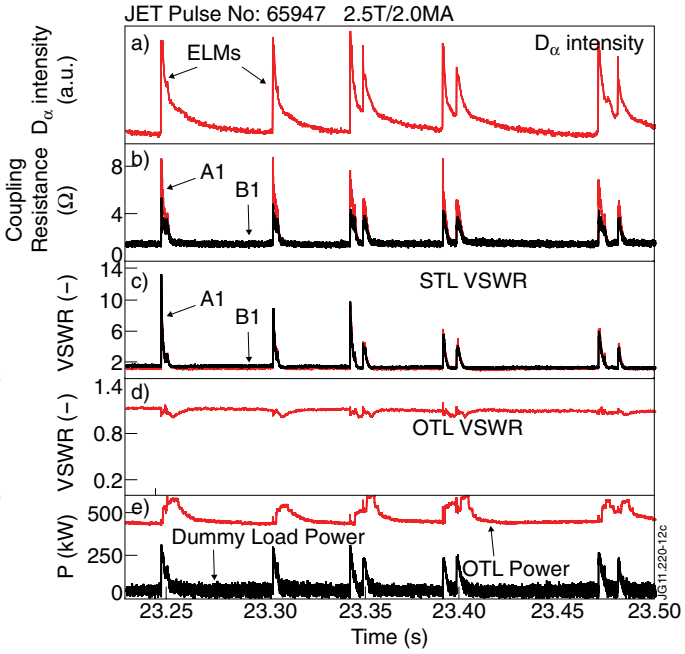

Figure 8: Example of the load tolerant system using 3dB hybrid Comparison of the power coupled to an ELMy plasma (i) by the 3dB system installed on antennas A and B and (ii) by the antennas C and D in the conventional configuration. The absence of trips by the protection system on antennas A and B leads to a significant increase in the average coupled power.

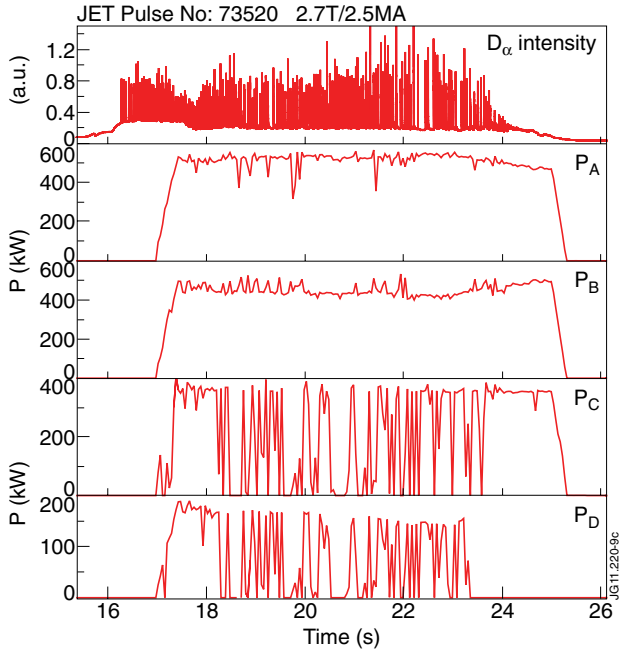

Figure 9: Comparison of the power coupled to an ELMy plasma (i) by the 3dB system installed on antennas A and B and (ii) by the antennas C and D in the conventional configuration. The absence of trips by the protection system on antennas A and B leads to a significant increase in the average coupled power.

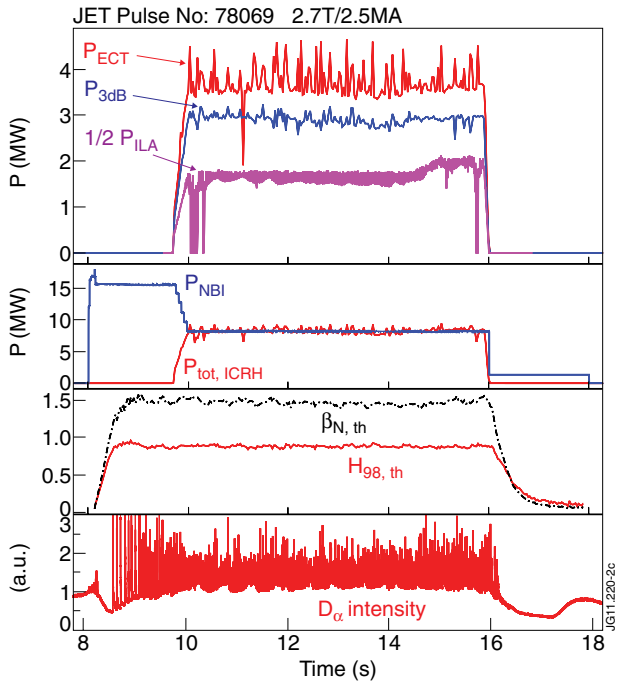

Figure 10: Simultaneous operation of ECT, 3dB and ILA in an ELMy H-Mode discharge. In the first 2s the total additional power consists of 15MW NBI power. This is subsequently equally split between 7.5MW ICRH and 7.5MW NBI. The thermal values of β_N and H_{98} show no significant difference between the two phases of the discharge.

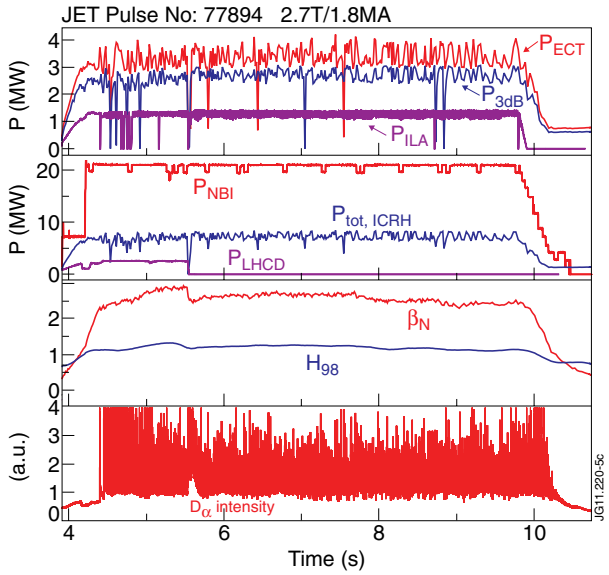

Figure 11: Time evolution of Advanced Mode Pulse No: 77894. Shown are from top to bottom (i) the coupled ICRH power from RCT, 3dB and ILA, (ii) the total heating powers from NBI, ICRH and LHCD, (iii) the normalized beta and confinement enhancement factor H_{98} and (iv) the D_α intensity characterizing the ELMs.

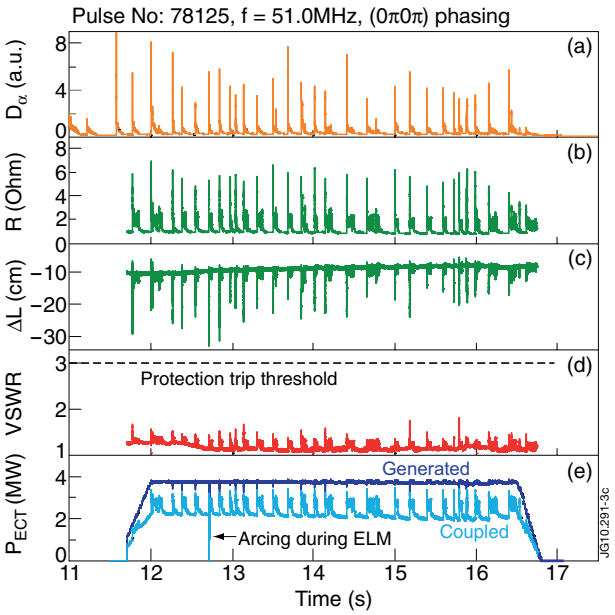

Figure 12: ECT behaviour during large ELMs: (a) mid-plane D_α line emission intensity, (b) antenna strap coupling resistance, (c) antenna strap equivalent length deviation from the vacuum value, (d) VSWR at amplifier output, (e) ICRF power generated and coupled. Plots (b), (c) and (d) are averaged values over the 4 ECT circuits; 5μs RF data sampling.

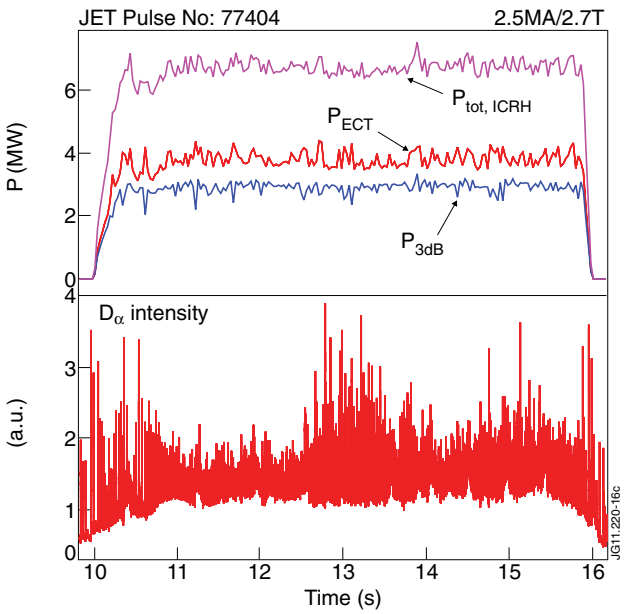

Figure 13: Example of the simultaneous operation of the 3dB system on antennas A and B and the ECT system on antennas C and D leading to high stationary values of the coupled ICRH power in ELMy H-mode plasmas on JET.

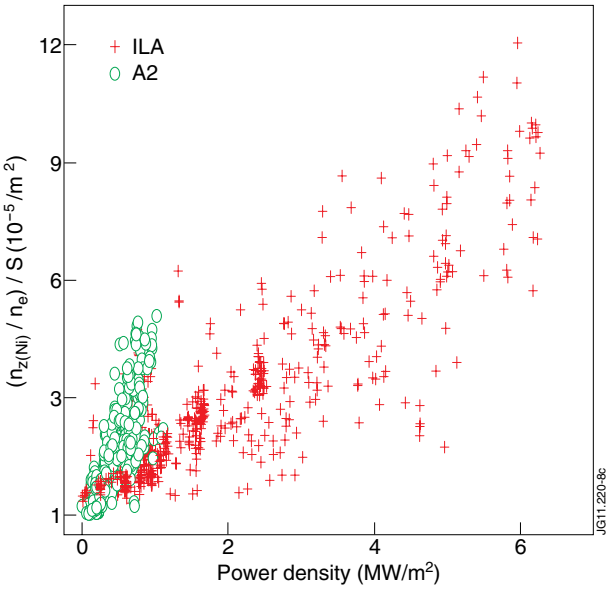

Figure 14: Correlation between Ni concentration (r/a ≈ 0.5–0.6) (normalized to the total strap surface of the A2 resp. ILA antenna, obtained with the horizontal VUV spectrometer (KT2), for the ILA (+) and the four A2 (o) antennas as function of the total ICRF power density at the antenna.

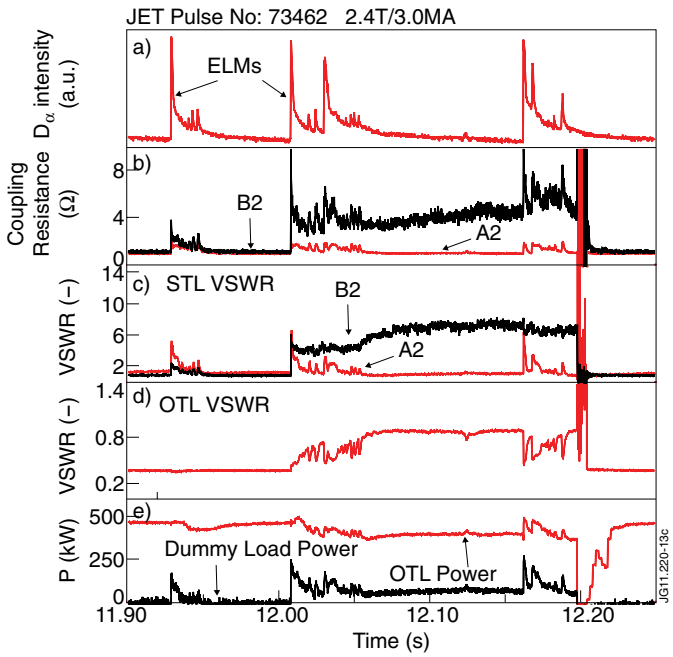

Figure 15: Example of a missed arc by the protection system for the load tolerant system using the 3dB hybrid couplers. Shown are as a function of time, from top to bottom: (a) Dα signal, (b) coupling resistance, (c) VSWR in the STLs connected to strap 2 of Antenna A and B, (d) VSWR in the OTL and (e) power in the OTL and directed to the dummy load.

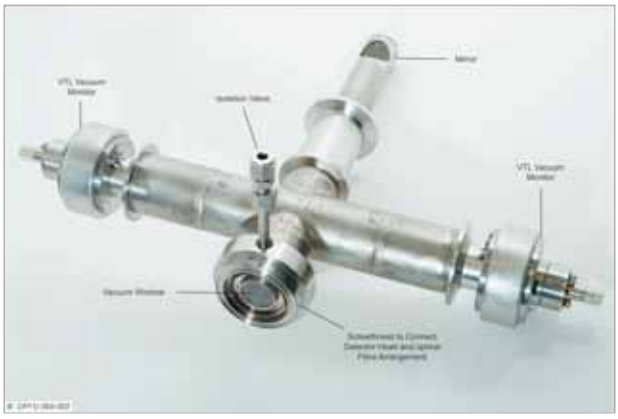

Figure 16: Spare detector showing the vacuum window, VTL pumping and mirror used in tests to assess why the installed VTL optical arc detection system failed.

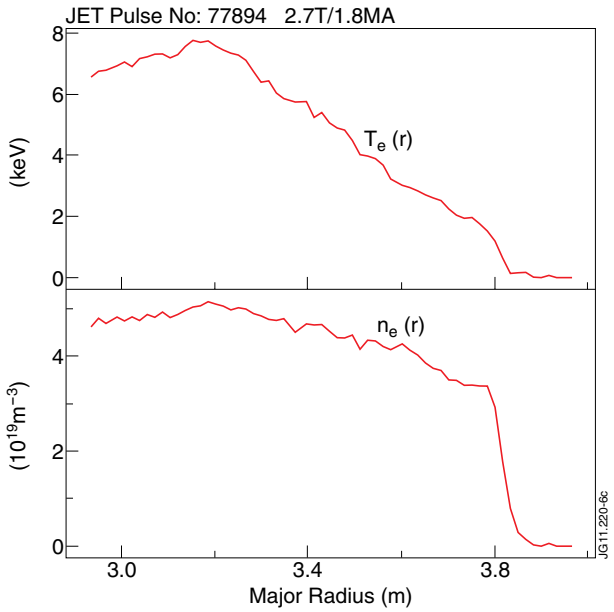

Figure 17: Profiles of electron temperature and density of Pulse No: 77894 at maximum performance. (averaged between 45.0 and 45.5s).